

Nanoscale

Accepted Manuscript



This is an *Accepted Manuscript*, which has been through the Royal Society of Chemistry peer review process and has been accepted for publication.

Accepted Manuscripts are published online shortly after acceptance, before technical editing, formatting and proof reading. Using this free service, authors can make their results available to the community, in citable form, before we publish the edited article. We will replace this *Accepted Manuscript* with the edited and formatted *Advance Article* as soon as it is available.

You can find more information about *Accepted Manuscripts* in the [Information for Authors](#).

Please note that technical editing may introduce minor changes to the text and/or graphics, which may alter content. The journal's standard [Terms & Conditions](#) and the [Ethical guidelines](#) still apply. In no event shall the Royal Society of Chemistry be held responsible for any errors or omissions in this *Accepted Manuscript* or any consequences arising from the use of any information it contains.



Journal Name

ARTICLE

Stable, polymer-directed and SPION-nucleated magnetic amphiphilic block copolymer nanoprecipitates with readily reversible assembly in magnetic fields.

Received 00th January 20xx,
Accepted 00th January 20xx

DOI: 10.1039/x0xx00000x

www.rsc.org/

Marco Giardiello,^a Fiona L. Hatton,^a Rebecca A. Slater,^a Pierre Chambon,^a Jocelyn North,^a Anita K. Peacock,^a Tao He,^b Tom O. McDonald,^a Andrew Owen,^c and Steve P. Rannard^{a,*}

The formation of inorganic-organic magnetic nanocomposites using reactive chemistry often leads to a loss of super-paramagnetism when conducted in the presence of iron oxide nanoparticles. We present here a low energy and chemically-mild process of co-nanoprecipitation using SPIONs and homopolymers or amphiphilic block copolymers, of varying architecture and hydrophilic/hydrophobic balance, which efficiently generates near monodisperse SPION-containing polymer nanoparticles with complete retention of magnetism, and highly reversible aggregation and redispersion behaviour. When linear and branched block copolymers with inherent water-solubility are used, a SPION-directed nanoprecipitation mechanism appears to dominate the nanoparticle formation presenting new opportunities for tailoring and scaling highly functional systems for a range of applications.

Introduction

In recent years, super-paramagnetic iron oxide nanoparticles (SPIONs) encapsulated into organic nanostructures have attracted considerable research interest in a broad range of scientific disciplines; including materials science, chemistry, biology and medicine.¹⁻⁵ The potential scope of biomedical applications of such inorganic-organic nanocomposites is extremely broad, and includes diagnostics, controlled drug delivery, magnetic fluid hyperthermia^{5b} for cancer therapy and imaging modalities such as magnetic resonance imaging (MRI) and the emerging magnetic particle imaging (MPI).⁶ Nanosystems loaded with super-paramagnetic iron oxide nanoparticles (SPIONs) of maghemite (γ - Fe_2O_3) and magnetite (Fe_3O_4) are of particular interest due to their relatively low toxicity and sensitivity to oxidation.⁷ Additionally, the preparation of organically protected SPIONs provides strategies to prevent the phagocytosis and clearance by macrophages of the mononuclear phagocyte system (liver, spleen, lungs and bone marrow) after intravenous injection.^{1,8} Colloidal stability is also essential within various applications and during storage; both resistance to aggregation and

enhancement of biocompatibility of magnetic particles is also improved by the use of organic stabilisers. Novel amphiphilic linoleic acid-modified chitosan nanoparticles containing multiple 12 nm SPION particles have recently been reported through a simple sonication in water with diameters ranging from 50 - 100 nm, showing accumulation in hepatocytes and offering good MRI contrast.⁹ Small molecule stabilising agents for SPIONs are known to desorb with decreasing concentration and lead to dilution-driven aggregation, whereas charged block-copolymer electrolytes have been reported to provide stabilisation to oleate-coated SPIONs in dilute dispersions and mediate the density of large aggregates on the micron-scale.¹⁰

Our research has focused on various polymers of complex architecture and their nanoprecipitation to yield monodisperse polymer nanoparticles with variable surface chemistries.¹¹⁻¹³ In recent years, we have observed that branched polymer nanoparticles can yield highly stable nanoprecipitates and the incorporation of polyethylene glycol (PEG)-derived initiators, within their controlled radical synthesis, leads to excellent stability under various environmental conditions.^{11,12} We have also described the synthesis of triple component inorganic-organic nanocomposite particles, with SPION encapsulation into solid organic polymer nanoparticles *via* a simple freeze drying/emulsion templating technique.¹⁴ Herein, a novel, low-energy and mild nanoprecipitation approach to SPION-loaded polymer nanoparticles is described, that efficiently encapsulates significant quantities of SPIONs. The impact of polymer architecture and hydrophilic-hydrophobic ratio is evaluated using a library of linear and highly branched amphiphilic block copolymers. The formation of nanocomposite particles appears to occur by either a polymer-directed or SPION-directed nucleation mechanism, depending

^a Department of Chemistry, University of Liverpool, Crown Street, L697ZD, UK.
E-mail: srannard@liverpool.ac.uk

^b Institute of Chemical and Engineering Sciences Agency for Science, Technology and Research (A*STAR), 1, Pesek Road, Jurong Island, 627833, Singapore.

^c Department of Molecular and Clinical Pharmacology, University of Liverpool, Block H, 70 Pembroke Place, Liverpool L69 3GF, UK

*Electronic Supplementary Information (ESI) available: Additional experimental details, NMR spectra, GPC chromatograms, kinetics experiments, graphs of nanoprecipitate aggregation and cycling studies and SPION characterisation See DOI: 10.1039/x0xx00000x

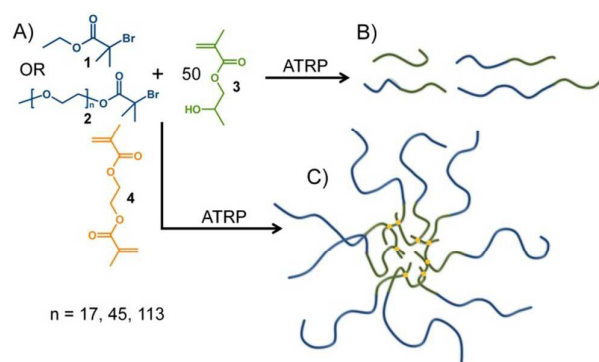
on selection of materials to yield uniform, highly SPION-loaded nanoparticles with excellent and rapid reversible aggregation under the influence of magnetic fields.

Results and discussion

Design and synthesis of amphiphilic A-B linear and branched block copolymers and super-paramagnetic iron oxide nanoparticles

Our previous reports of the synthesis of branched and linear polymers, utilising atom transfer radical polymerisation (ATRP), have utilised the commercially available tertiary bromide initiator ethyl-2-bromo isobutyrate (EBIB; **1**). As with many other groups, we have also utilised PEG-macroinitiators (PEG-Br; **2**) of varying number average degrees of polymerisation (DP_n) for ATRP.¹⁵⁻¹⁷ Within this study, PEG-macroinitiators with 17, 45 and 113 ethylene oxide repeat units were selected, corresponding to molecular weights of 750, 2000 and 5000 g/mol respectively. The hydrophilic monomer 2-hydroxypropyl methacrylate (HPMA; **3**) has been successfully used to form branched polymers that yield stable nanoprecipitates. HPMA forms hydrophobic p(HPMA) upon polymerisation and acts as a poorly water-soluble block segment within the target amphiphilic block copolymers; the inclusion of a low concentration of ethylene glycol dimethacrylate (EGDMA; **4**) allows branching between chains during propagation when desired (Scheme 1). A detailed synthetic description can be found in the Electronic Supporting Information (ESI Fig. S1-S7)

HPMA was polymerised under methanolic conditions to a target $DP_n = 50$ monomer units for each of the chosen polymer structures, reaching >99% conversion in each case and generating a library of materials that varied in PEG chain length and architecture. The linear polymers were characterised using triple detection size exclusion chromatography (SEC), showing unimodal molecular weight distributions, whilst the well-reported high molecular weight multimodal distributions indicative of statistical branching were seen for polymerisations containing EGDMA (ESI Fig. S5-6).



Scheme 1: Schematic representation of the methanolic atom transfer radical polymerisation of linear and branched homopolymers and A-B block copolymers. A) Variation of initiators with either ethyl, **1**, or various PEG_n, **2**, functionalities; B) linear polymer structures with varying hydrophilic block length at constant p(HPMA)₅₀; and C) inclusion of EGDMA, **4**, forming branched polymers (idealised structure of p(PEG₁₁₃-b-(HPMA₅₀-co-EGDMA_{0.95})) shown)

Good targeting of number average molecular weights (M_n) was also seen for the linear polymers, and high dispersities (\mathcal{D}) and weight average molecular weight (M_w) values were obtained for branched analogues (Table 1).

Oleic acid coated SPIONs were prepared following previously reported thermal decomposition routes.¹⁸ Briefly, an iron (III) oleate complex precursor was prepared by refluxing iron (III) chloride hexahydrate and sodium oleate at 70 °C in a mixture of deionised water, ethanol and hexane for 4 hours. The iron (III) oleate complex was then isolated and dissolved in 1-octadecene and heated at 320 °C for 30 minutes. Upon cooling, and following addition of cold ethanol, the pure SPIONs precipitated. Importantly, the SPIONs were aggregated using a strong NdFeB magnet and the ethanol decanted and replaced with tetrahydrofuran (THF) with subsequent SPION redispersion; THF is a good solvent for the polymers outlined in Table 1 and, therefore, the solvent of choice for co-nanoprecipitation studies as it is water-miscible and results in no dissolution of the SPION oleic acid stabilisers. The ability to magnetically aggregate and re-disperse the SPIONs is also of great use as it demonstrates their surface stability and lack of magnetic agglomeration of the super-paramagnetic metallic oxide nanoparticles under organic solvent conditions. The SPIONs may contain a mixture of Fe₃O₄ and γ-Fe₂O₃ (ESI Fig. S8-15) and were characterised by infrared spectroscopy (FT-IR), thermal gravimetric analysis (TGA), powder x-ray diffraction (pXRD) and dynamic light scattering (DLS), strongly matching previous reports.¹⁸

Table 1: Triple detection size exclusion chromatography analysis of linear and branched polymer and copolymer library generated for this study.

Polymer ^a	M_n g/mol (Theory)	M_n g/mol (SEC) ^b	M_w g/mol (SEC) ^b	\mathcal{D} (SEC) ^b	Weight Av. # of chains ^c
p(HPMA ₅₀)	7200	11250	13950	1.24	1
p(PEG ₁₇ -b- HPMA ₅₀)	8000	8100	9800	1.21	1
p(PEG ₄₅ -b- HPMA ₅₀)	9200	10000	12000	1.20	1
p(PEG ₁₁₃ -b- HPMA ₅₀)	12200	13300	16800	1.26	1
p(HPMA ₅₀ -co- EGDMA _{0.8})	-	147,100	928,500	6.31	67
p(PEG ₁₇ -b- HPMA ₅₀ -co- EGDMA _{0.95})	-	57200	150,400	2.63	15
p(PEG ₄₅ -b- HPMA ₅₀ -co- EGDMA _{0.95})	-	43300	110,400	2.55	9
p(PEG ₁₁₃ -b- HPMA ₅₀ -co- EGDMA _{0.95})	-	45400	118,500	2.61	7

^aNominal target DP_n values used to name polymers - all polymers synthesised by Cu(I)Cl/bpy catalysed ambient temperature methanolic ATRP; ^bTriple detection SEC using THF eluent containing 2 v/v % of triethylamine; ^cWeight average number of conjoined chains within each sample calculated by (M_w (SEC) of branched polymer/ M_w (SEC) of linear equivalent polymer)

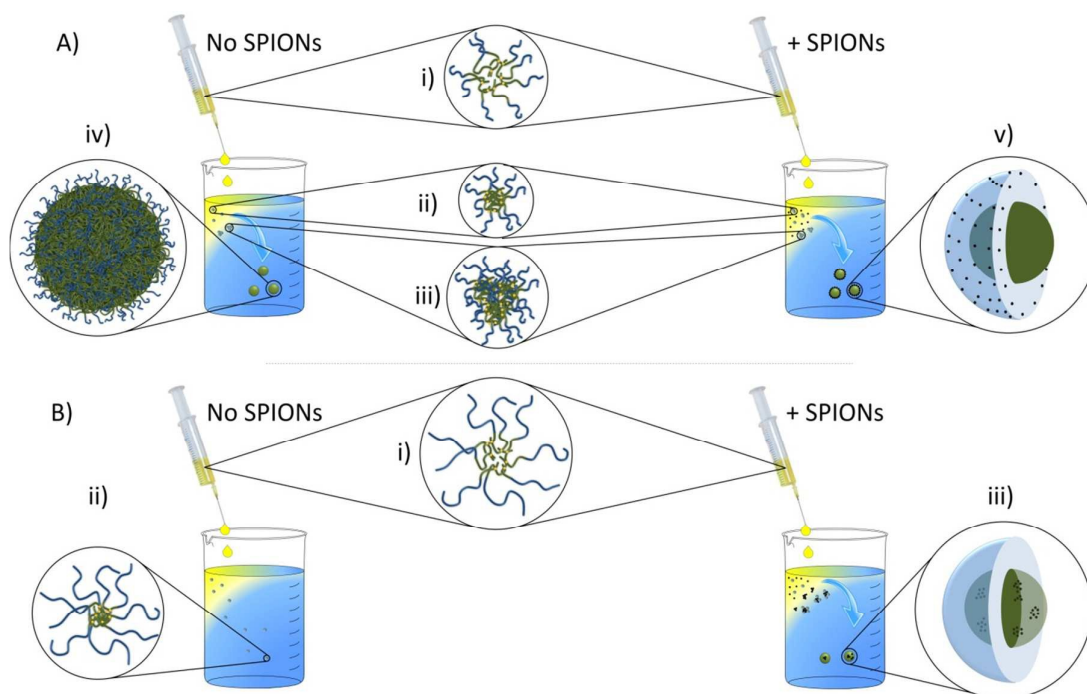


Figure 1: Schematic representation of SPION-containing composite nanoprecipitate formation showing the branched polymer case. A): i) solvated polymer (able to nanoprecipitate) added to water with ii) collapse of polymer to form nuclei which iii) aggregate to form iv) stable self-assembled nanoparticles. In the presence of SPIONs, the magnetic nanoprecipitates v) contain SPIONs predominantly surrounding the polymer nuclei. B): i) polymer solutions (high degree of hydrophilicity) form ii) un-assembled collapsed structures when added to water in the absence of SPIONs, but the presence of SPIONs leads to iii) nanoprecipitates containing domains of SPIONs that have nucleated the co-nanoprecipitation.

pXRD determined the crystal diameter as 8.05 ± 1.79 nm while DLS showed an hydrodynamic diameter (D_z) = 27 ± 2 nm, number average diameter (D_n) = 18 ± 2 nm, volume average diameter (D_v) = 21 ± 2 nm and Pdl = 0.23. Thermal gravimetric analysis (TGA) showed the inorganic/bound organic component ratio to be 1:1.1 (ESI Fig. S11) and the concentration was determined as 7.24 mg/mL with respect to SPION (15.27 mg/mL total mass, including oleic acid). SPION magnetisation was determined using a super-conducting quantum interference device (SQUID) as 43.61 emu/g (ESI Fig. S14).

Co-nanoprecipitation of branched and linear polymers in the absence and presence of SPIONs

The formation of magnetic inorganic–organic polymer nanocomposites has been achieved using a number of techniques such as SPION surface initiation of polymerisation^{19–21} and encapsulation via miniemulsion polymerisation²². Such techniques have been shown to reduce the super-paramagnetism of the SPIONs within the resulting nanocomposite structures and require multiple washing steps during isolation of the purified products from reaction media and unreacted monomer. Loss of SPION magnetisation is assumed to be derived from the oxidising and thermally aggressive initiation/polymerisation conditions and the processing of mini-emulsions using ultra-sonication. Nanoprecipitation is a low-energy process that is postulated to

utilise a nucleation-aggregation mechanism after a solvent switch from a good solvent into a miscible anti-solvent.²³ We have recently observed this phenomena during the slow addition of hexane (anti-solvent) to an acetone (good solvent) solution of highly branched hydrophobic polymers, identifying the formation of swollen self-assembled/aggregated nanoparticles after the nucleation of small collapsed structures.²⁴ For poorly water-soluble polymers, nanoprecipitation is often conducted by drop-wise or rapid addition of polymer solutions, in water-miscible good solvents, directly into water (acting as the anti-solvent). The prevention of macro-phase separation is accomplished by the rapid achievement of either steric or charge stabilisation (or a combination of both) during the formation of the resulting nanoparticles.¹¹ Such stabilisation may be derived from charged end groups,²⁵ the presence and adsorption of added surfactants or the co-nanoprecipitation of stabilising polymer components which are integrated into the nanoparticle.¹⁵

A co-nanoprecipitation approach of inorganic and organic components was adopted in this study to promote the incorporation of SPIONs into a polymeric nanoparticle, using the self-assembly of polymers during the solvent switch. In all cases, a SPION content of 10% w/w was targeted (note; loadings are calculated on inorganic content only and not the combined mass of inorganic components and oleic acid stabiliser). The eight polymers in Table 1 were individually dissolved in THF to a final concentration of 5 mg/mL.

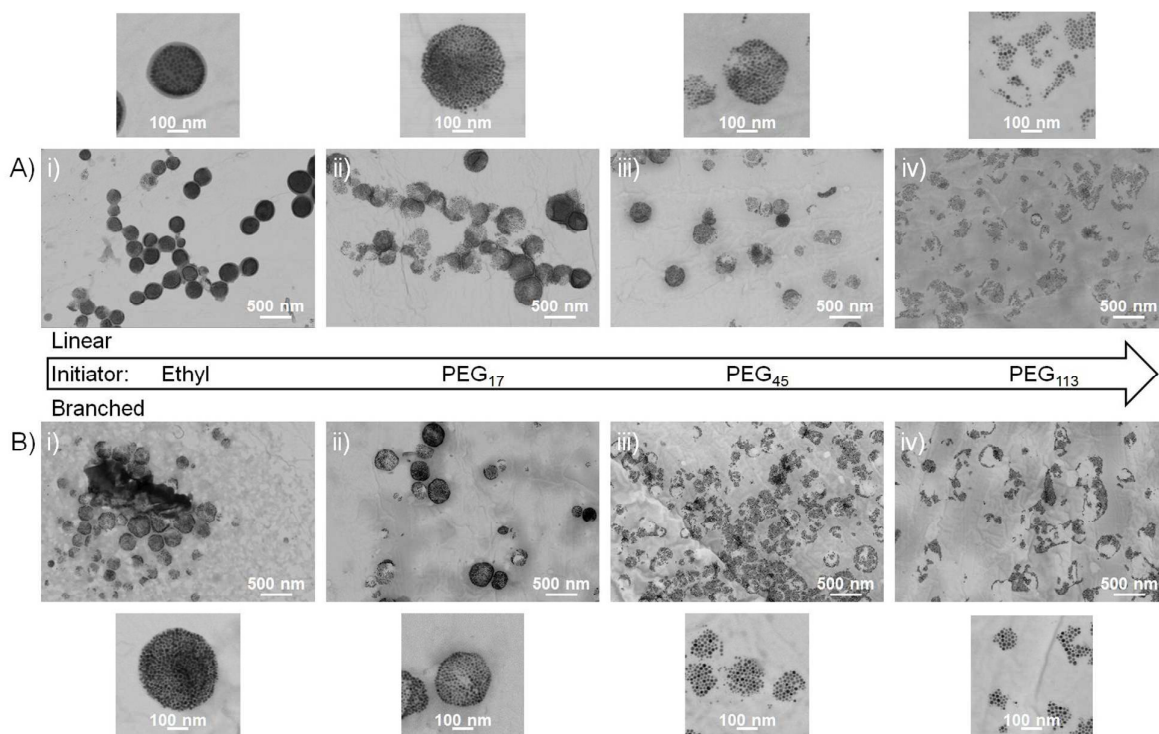


Figure 2: Transmission electron microscopy of linear and branched polymer co-nanoprecipitates formed in the presence of SPIONs. A) Well defined structures with SPIONs located predominantly at the surface of nanoparticles comprising i) $p(\text{HPMA}_{50})$ and ii) $p(\text{PEG}_{17}\text{-}b\text{-}(\text{HPMA}_{50}))$; increasingly poorly-defined SPION domains with increasing polymer hydrophilicity showing SPION-directed nucleation of iii) $p(\text{PEG}_{45}\text{-}b\text{-}\text{HPMA}_{50})$ and iv) $p(\text{PEG}_{113}\text{-}b\text{-}\text{HPMA}_{50})$. B) Similar well defined structures from the branched copolymers i) $p(\text{HPMA}_{50}\text{-}co\text{-}\text{EGDMA}_{0.8})$ and ii) $p(\text{PEG}_{17}\text{-}b\text{-}(\text{HPMA}_{50}\text{-}co\text{-}\text{EGDMA}_{0.95}))$ leading to SPION-directed nucleation in the presence of iii) $p(\text{PEG}_{45}\text{-}b\text{-}(\text{HPMA}_{50}\text{-}co\text{-}\text{EGDMA}_{0.95}))$ and $p(\text{PEG}_{113}\text{-}b\text{-}(\text{HPMA}_{50}\text{-}co\text{-}\text{EGDMA}_{0.95}))$. Additional images show higher magnification of each sample.

Within the co-nanoprecipitation process, 1 mL of the polymer/THF solution (5 mg polymer) was rapidly added to 5 mL of water and immediately followed by 69 μL of the SPION/THF dispersion (0.5 mg SPION at 7.24 mg/mL). During control experiments in the absence of SPIONs, 69 μL of pure THF was added at this stage to ensure equivalent good solvent/anti-solvent volumes. The mixtures were allowed to stir overnight to ensure removal of THF via evaporation (Fig. 1).

Following solvent removal, the resulting 5 mL nanoparticle dispersions contained either 1 mg/mL of polymer (control experiments) or 1.1 mg/mL of nanocomposite material (1 mg/mL of polymer + 0.1 mg/mL SPIONs). Dynamic light scattering (DLS) was used to characterise the resulting products (Table 2) with scanning and transmission electron microscopy (SEM and TEM) chosen to investigate a range of samples (Fig. 2&3). In the absence of SPIONs, DLS confirmed our earlier studies that despite the successful nanoprecipitation of linear $p(\text{HPMA}_{50})$ initiated from EBiB, the product nanoprecipitates were large and relatively polydisperse. This was clear when comparing to outcomes when using the equivalent branched polymer $p(\text{HPMA}_{50}\text{-}co\text{-}\text{EGDMA}_{0.8})$, generating near-monodisperse nanoprecipitates of approximately 20% of the D_z of the nanoparticles resulting from the linear material, Table 2. A similar trend was seen for

PEG_{17} -initiated linear and branched polymers where a decrease in size and PDI was again seen when nanoprecipitating the branched architectures. As the hydrophilic-hydrophobic balance is increased in favour of the hydrophilic block segment, via increasing PEG initiator DP_n , the linear and branched A-B block copolymers formed solutions with very poor scattering, implying that limited self-assembly of the collapsed hydrophobic polymer segments (branched or linear) was occurring during the solvent switch (Table 2).

When THF dispersions of SPIONs are added to the anti-solvent immediately after initial addition of the polymer solution, a different behaviour was observed. The addition of SPIONs prior to full solvent removal resulted in nanoprecipitate formation across the full series of linear polymers of $p(\text{HPMA}_{50})$ and $p(\text{PEG}_x\text{-}b\text{-}\text{HPMA}_{50})$ studied, Table 2. Additionally, a general trend towards smaller particles and decreasing polydispersity was also seen with increasing chain length of the PEG block segment. The addition of SPIONs to the nanoprecipitation of branched polymer largely mirrored the behaviour of the linear homo- and A-B block copolymers although a number of key differences were observed. Firstly, SPION addition led to larger nanoprecipitates for the branched polymer initiated by EBiB and, although a trend of decreasing D_z was seen with increasing PEG chain length, a much smaller

difference in the diameters of nanoprecipitates of branched A-B block copolymers in the presence of SPIONs was seen.

Table 2 Dynamic light scattering analysis of polymer nanoprecipitation experiments in the presence and absence of SPIONs and control experiment of SPIONs in the absence of polymer

Polymer/Sample	-SPION			+SPION		
	D_z (nm)	D_n (nm)	Pdl	D_z (nm)	D_n (nm)	Pdl
$p(\text{HPMA}_{50})$	510	360	0.26	280	240	0.21
$p(\text{PEG}_{17}\text{-}b\text{-HPMA}_{50})$	670	520	0.22	365	220	0.25
$p(\text{PEG}_{45}\text{-}b\text{-HPMA}_{50})$	-	-	-	225	185	0.13
$p(\text{PEG}_{113}\text{-}b\text{-HPMA}_{50})$	-	-	-	175	145	0.09
$p(\text{HPMA}_{50}\text{-CO-EGDMA}_{0.8})$	110	85	0.08	310	270	0.14
$p(\text{PEG}_{17}\text{-}b\text{-}(\text{HPMA}_{50}\text{-CO-EGDMA}_{0.95}))$	49	30	0.17	195	70	0.24
$p(\text{PEG}_{45}\text{-}b\text{-}(\text{HPMA}_{50}\text{-CO-EGDMA}_{0.95}))$	-	-	-	180	140	0.12
$p(\text{PEG}_{113}\text{-}b\text{-}(\text{HPMA}_{50}\text{-CO-EGDMA}_{0.95}))$	-	-	-	165	135	0.07
Oleic acid – stabilised SPIONs ^a	-	-	-	310	265	0.17

^aNanoprecipitation in the absence of polymer.

As a control experiment, SPIONs were nanoprecipitated directly in the absence of polymer, forming aggregates with a $D_z = 310$ nm under these conditions, however, these dispersions were not stable and macrophase separation was observed after < 24 hours. All polymer-SPION nanoprecipitates were stable for extended periods (minimum of 4 weeks) as aqueous dispersions in deionised water.

The SPION-induction of nanoprecipitation for linear and branched A-B block copolymers initiated with PEG₄₅ and PEG₁₁₃ was clearly of interest, suggesting a different mechanism to nanoparticle formation than that seen for polymers capable of self-assembly in the absence of SPIONs. TEM analysis (Fig. 2) of nanoprecipitates derived from PEG-free polymers or polymers containing PEG₁₇ chains appeared to show a high density of SPIONs arranged around a largely SPION-free polymer core and adopting a spherical arrangement. As the PEG chain length increased to 45 and 113 monomer units, the definition of the SPION arrangement decreased considerably and smaller, relatively randomly-shaped SPION clusters were observed.

The observed nanoprecipitation of SPIONs in the absence of polymer supports the SPION-induced nucleation of nanoprecipitation in the presence of A-B copolymers unable to nanoprecipitate conventionally; the A-B copolymers also provide stabilisation. Cryo-TEM of the SPION-induced nanoprecipitates incorporating $p(\text{PEG}_{113}\text{-}b\text{-}(\text{HPMA}_{50}\text{-CO-EGDMA}_{0.95}))$, also confirmed separated SPION clusters and suggests that the TEM images shown from dried samples are not derived from drying effects (Fig. 3Aiii and iv). In all cases, no un-encapsulated SPIONs were seen within the TEM studies.

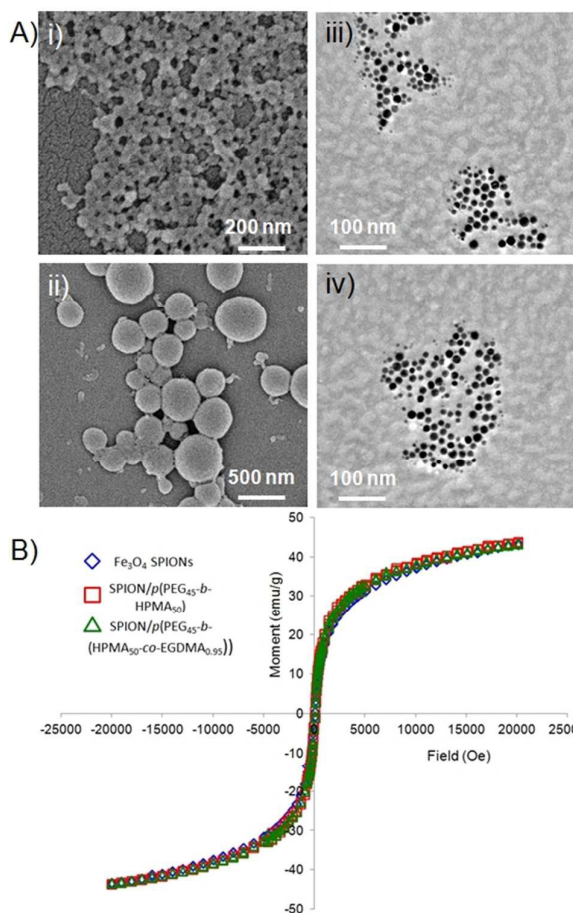


Figure 3: Analysis of nanoprecipitated particles. A) SEM images of i) nanoprecipitates of $p(\text{HPMA}_{50}\text{-CO-EGDMA}_{0.8})$ in the absence of SPIONs and ii) nanoprecipitates of $p(\text{HPMA}_{50})$ in the presence of SPIONs, and cryo-TEM images of iii-iv) SPION nuclei within nanoprecipitates containing $p(\text{PEG}_{45}\text{-}b\text{-}(\text{HPMA}_{50}\text{-CO-EGDMA}_{0.95}))$. B) overlaid comparative SQUID analysis of freshly prepared SPIONs (blue diamonds) and SPION containing polymer nanoprecipitates containing linear $p(\text{PEG}_{45}\text{-}b\text{-HPMA}_{50})$ (red squares) and branched $p(\text{PEG}_{45}\text{-}b\text{-}(\text{HPMA}_{50}\text{-CO-EGDMA}_{0.95}))$ (green triangles).

The stabilisation, and arrest of SPION-polymer composite nanoprecipitate growth, is attributable to the steric repulsion of the PEG-chains associated with the A-B block copolymers. The extended coil length of a PEG₁₇ chain, tethered at one chain end, is estimated to be approximately 1 nm, whilst PEG₄₅ and PEG₁₁₃ are estimated to be 3 nm and 6 nm respectively. In molecular dynamics studies of PEG-conjugated PAMAM dendrimers with increasing numbers of surface PEG chains, the thickness of the PEG layer was seen to increase with increasing conjugation density.²⁶ As the PEG-containing nanoprecipitates are essentially neutral, a purely steric stabilisation is expected. The presence of an increasing number of varying PEG chains during the growth stages of the nanoprecipitation will lead to colloidal stability being attained at different D_z values; lower diameters achieved for longer PEG chain lengths. As shown previously, nanoprecipitation of linear and branched $p(\text{HPMA}_x)$ leads to highly negatively charged nanoparticles and a purely charge-stabilisation mechanism is expected in these cases.

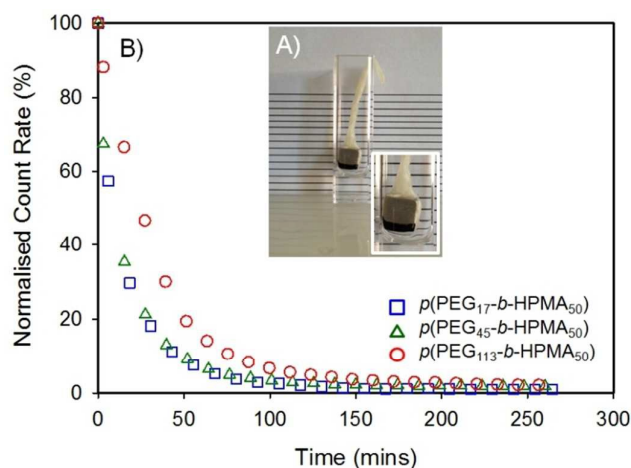


Figure 4: Illustrative example of studies of magnetic nanoprecipitate response to applied magnetic fields. A) Aggregation of nanoprecipitates at a suspended NdFeB magnet surface and B) monitoring of normalised count rate, measured by DLS, during the aggregation process. Data shown for SPION-containing nanoprecipitates comprising linear A-B block copolymers of varying PEG chain length. Comparative graphs for branched polymers are shown in the Electronic Supporting Information.

We have previously compared the nanoprecipitation of a range of branched copolymers and consistently reported lower D_z and Pdl values when branched polymers are self-assembled in this way. The multiple chains that are conjoined within the distribution of branched architectures may modify the kinetics of the stabilisation process by involving the concerted association of numerous chains rather than an individual chain-by-chain aggregation process.

Reversible aggregation and salt stability of SPION-containing nanoprecipitates

Before studies of the aggregation of SPION-polymer composite nanoprecipitates under magnetic fields, SQUID analysis was performed on two representative samples produced using the linear and branched block copolymers with PEG_{45} chains and compared to the SPIONs as synthesised (Fig. 3B). The magnetisation values of the nanoprecipitated composites were, within error, identical to the starting SPIONs; the three values ranged between 43.51-43.90 emu/g, demonstrating the mild processing conditions.

Aggregation studies were conducted by monitoring the scattering count rate of dispersions placed within the DLS instrument in the presence of a strong NdFeB magnet suspended over the sample and in direct contact with the liquid surface (Fig. 4A). The magnet was suspended above the liquid to prevent measurements being affected by sedimentation, the attenuator was maintained at a constant value and measurements were taken regularly over 5 hours (Fig. 4B). A significant and rapid decrease in count rate was observed for all SPION-containing nanoprecipitates leading to values that were insufficient for accurate size measurement. D_z and D_n values also decreased during the experiment, probably due to the varying density of SPIONs within each size distribution leading to larger or more SPION-rich particles

being removed faster than other, less magnetic nanoparticles. The time taken to decrease to < 20 % of the starting count rate was studied. This value typically equated to the point where size measurements were no longer reliable and indicated the effective point of nanoprecipitate removal.

In general, nanoprecipitates comprising branched polymers showed a steeper gradient of decreasing count rate than those comprised of their linear polymer analogues (Table S1), although in several cases the differences were marginal. Many nanoprecipitates were effectively removed from the dispersion in less than 30 minutes with the greatest difference being seen for branched and linear polymers initiated by PEG_{113} (36 mins and 50 mins respectively). After aggregation, the nanoprecipitates readily redispersed with gentle manual shaking, leading to a detailed study of the reversibility of aggregation after prolonged exposure to the magnetic field (Fig. 5; ESI Fig. S21&22). In each experiment, nanoprecipitates were aggregated to a magnet placed at the side of the DLS cuvette overnight (> 16 hours), after which the magnet was removed and analysis by DLS allowed count rates to be measured; in almost all cases, these were extremely low or non-detectable.

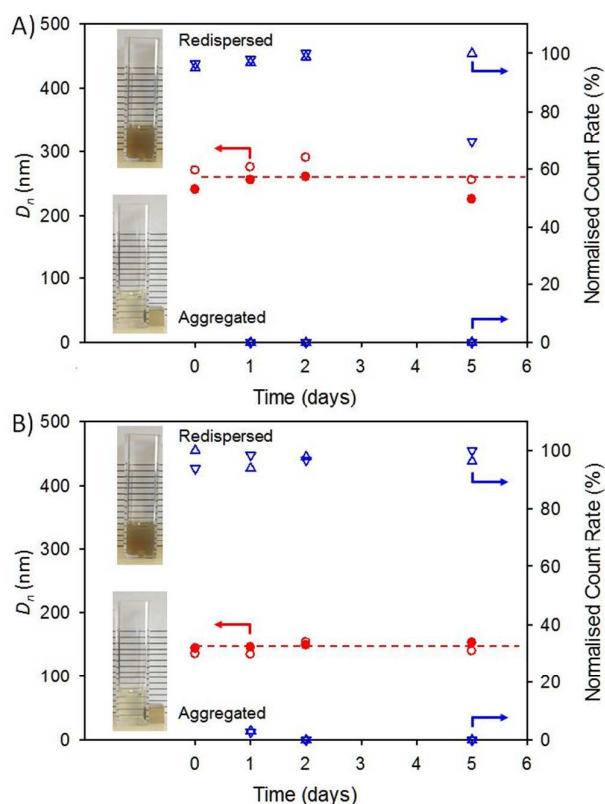


Figure 5: Illustrative examples of DLS studies of reversible aggregation and re-dispersion of SPION-containing nanoprecipitates comprising A) linear $p(\text{HPMA}_{50})$ (blue inverted triangles/filled red circles) and branched $p(\text{HPMA}_{50}\text{-}co\text{-EGDMA}_{0.8})$ (blue triangles/open red circles) and B) linear $p(\text{PEG}_{113}\text{-}b\text{-HPMA}_{50})$ (blue inverted triangles/filled red circles) and branched $p(\text{PEG}_{113}\text{-}b\text{-}(\text{HPMA}_{50}\text{-}co\text{-EGDMA}_{0.95}))$ (blue triangles/open red circles). Data shows three cycles of aggregation and re-dispersion over five days and resulting normalised count rates for both aggregated or re-dispersed samples and D_n values of re-dispersed samples.

The aggregated nanoparticles were very responsive to movements in the magnetic field (Movie S1). Gentle manual agitation for less than 60 seconds (Movie S2) led to no observable remaining aggregates and DLS measurement was again conducted to establish D_z , D_n and count rate values. This aggregation-redispersion cycle was repeated twice (over 2 days) before re-aggregating the nanoparticles and redispersing after 72 hours under the influence of the magnetic field. In every case, the samples re-dispersed easily and yielded near identical DLS measurements (Fig 5; ESI Fig. S21&22) to the initial values. SPION-containing nanoprecipitates formed from the branched polymers generally redispersed to present the highest count rates after prolonged and repeated aggregation/redispersion cycles, although differences were relatively small between the analogous polymer architectures.

The application of magnetic nanoparticles often requires complex electrolyte environments. To study the effect of salt on the aqueous nanoparticle dispersions, the eight polymer-SPION nanoprecipitates and the SPION-only nanoprecipitate were subjected to addition of 0.5M NaCl (200 μ L to 1 mL of aqueous nanoparticles at a concentration of 1 mg/mL; final NaCl concentration = 83 mM). Nanoprecipitates comprised of SPIONs alone, or containing linear and branched polymers initiated by EBiB or PEG₁₇ instantly aggregated with observable macro-phase separation. This is consistent with predominantly charge-stabilised structures; zeta potential (ζ) values of the nanoparticles prior to salt addition were indeed highly negative and ranged from -23 to -53 mV. Screening of surface potential by added electrolyte clearly limits the value of these materials, despite the polymer-directed nanoprecipitation mechanism and the efficient uptake of SPIONs yielding dense inorganic-organic composite nanoparticles.

Addition of salt to the nanoprecipitates bearing PEG₄₅ and PEG₁₁₃ chains led to an instant effect on the SPION-containing nanoparticles derived from the linear $p(\text{PEG}_{45}\text{-}b\text{-HPMA}_{50})$, with a 22% increase in observed D_z and 46% increase in D_n values. This change in observed size was not accompanied with visual phase separation but a concomitant decrease in ζ from -22 mV to -2 mV was seen. The nanoprecipitates derived from the branched equivalent $p(\text{PEG}_{45}\text{-}b\text{-}(\text{HPMA}_{50}\text{-CO-EGDMA}_{0.95}))$ displayed a negligible increase in D_z (2 nm) but a 27% increase in D_n values on salt addition (ζ decrease from -19 mV to -2 mV). The linear and branched polymer-containing nanoprecipitates with PEG₁₁₃ chains both showed < 3 nm variation in D_z or D_n values after addition of salt, but identical decreases in ζ to near neutral values (-3 mV).

The stability of the PEG₁₁₃-containing nanoprecipitates demonstrates the expected steric stabilisation from the long solvated block segments and also provides the potential for the use of these materials within complex biological environments, although this has not been established during this study.

Conclusions

The investigation of linear amphiphilic A-B block copolymers and their branched copolymer analogues in the rapid

formation of SPION-containing particles by co-nanoprecipitation has indicated two distinct mechanisms of formation; polymer-directed and SPION-directed self-assembly. This facile nanoprecipitation methodology is highly efficient, incorporating large quantities of SPIONs into the inorganic-organic nanocomposites. The low energy process exceeds the efficiency of more complex literature methods and avoids *in situ* chemical or polymerisation techniques which result in loss of super-paramagnetism of the encapsulated SPIONs.

The magnetic composite nanoprecipitates can be repeatedly manipulated by applied external magnetic fields maintaining particle integrity and properties whilst avoiding particle aggregation. Variation of polymer architecture and composition demonstrates the benefits of polymer design to maximise performance and offers potential models for medically relevant nanocomposites for *in vivo* imaging, targeted delivery of drugs or hyperthermia agents within cancer therapies.

Acknowledgements

The authors would like to acknowledge funding from the Engineering and Physical Research Council (EPSRC) for a vacation bursary (JN) and the EPSRC/University of Liverpool for PhD studentships for FLH, RAS and AP. Additional funding from EPSRC was available for this study from EPSRC (EP/G066272/1 and EP/K002201/1). The authors also thank Mr Ben Reed for aiding a series of experiments, the Centre for Materials Discovery for access to scanning and transmission electron microscopy and the A*STAR institutes for access to cryo-TEM.

Notes and references

- 1 D. K. Kim and J. Dobson, *J. Mater. Chem.*, 2009, **19**, 6294.
- 2 F. M. Kievit and M. Zhang, *Accounts Chem. Res.*, 2011, **44**, 853.
- 3 Q. A. Pankhurst, N. K. T. Thanh, S. K. Jones, J. Dobson, *J. Phys. D-Appl. Phys.*, 2009, **42**, 224001/1.
- 4 A. C. Balazs, T. Emrick, T. P. Russell, *Science*, 2006, **314**, 1107.
- 5 a) M. Lin, H. H. Kim, H. Kim, J. Dobson and D. K. Kim, *Nanomedicine-UK*, 2010, **5**, 109; b) Y. I. Golovin, S. L. Gribanovsky, D. Y. Golovin, N. L. Klyachko, A. G. Majouga, A. M. Master, M. Sokolsky, A. V. Kabanov, *J. Control. Release*, 2015, **219**, 43.
- 6 B. Gleich and R. Weizenecker, *Nature*, 2005, **435**, 1214
- 7 N. Tran and T. J. J. Webster, *J. Mater. Chem.*, 2010, **20**, 8760.
- 8 S. Mornet, S. Vasseur, F. Grasset and E. J. Duguet, *J. Mater. Chem.*, 2004, **14**, 2161.
- 9 C. M. Lee, H. J. Jeong, S. L. Kim, E. M. Kim, D. W. Kim, S. T. Lim, K. Y. Jang, Y. Y. Jeong, J. W. Nah and M. H. Sohn, *Int. J. Pharm.*, 2009, **371**, 163.
- 10 J. Hajduová, M. Uchman, I. Šafařík, M. Šafaříková, M. Šlouf, S. Pispas and M. Štěpánek, *Colloid Surface A*, 2015, **483**, 1.
- 11 H. E. Rogers, P. Chambon, S. E. R. Auty, F. Y. Hern, A. Owen, and S. P. Rannard, *Soft Matter*, 2015, **11**, 7005.
- 12 F. L. Hatton, L. M. Tatham, L. R. Tidbury, P. Chambon, T. He, A. Owen and S. P. Rannard, *Chem. Sci.*, 2015, **6**, 326.
- 13 R. A. Slater, T. O. McDonald, D. J. Adams, E. R. Draper, J. V. M. Weaver and S. P. Rannard, *Soft Matter*, 2012, **8**, 9816.

- 14 M. Giardiello, T. O. McDonald, P. Martin, A. Owen and S. P. Rannard, *J. Mater. Chem.*, 2012, **22**, 24744.
- 15 A. B. Dwyer, P. Chambon, A. Town, F. L. Hatton, J. Ford and S. P. Rannard, *Polym. Chem.*, 2015, **6**, 7286.
- 16 J. Ford, P. Chambon, J. North, F. L. Hatton, M. Giardiello, A. Owen and S. P. Rannard, *Macromolecules*, 2015, **48**, 1883.
- 17 S. Sugihara, K. Sugihara, S. P. Armes, H. Ahmad and A. L. Lewis, *Macromolecules*, 2010, **43**, 6321.
- 18 a) J. Park, K. An, Y. Hwang, J.G. Park, H. J. Noh, J.Y. Kim, J. H. Park, N.M. Hwang and T. Hyeon, *Nat. Mater.*, 2004, **3**, 891; b) A. K. Peacock, S. I. Cauet, A. Taylor, P. Murray, S. R. Williams, J. V. M. Weaver, D. J. Adams and M. J. Rosseinsky Chem. Commun., 2012, **48**, 9373.
- 19 W. H. Binder, D. Gloger, H. Weinstabl, G. Allmaier and E. Pittenauer, *Macromolecules*, 2007, **40**, 3097.
- 20 M. Lattuada and T. A. Hatton, *Langmuir*, 2007, **23**, 2158.
- 21 Q. L. Fan, K. G. Neoh, E. T. Kang, B. Shuteru and S. C. Wang, *Biomaterials*, 2007, **28**, 5426.
- 22 a) C. K. Weiss and K. Landfester, *Hybrid Latex Particles: Preparation with (Mini) Emulsion Polymerization*, ed. A. M. Van Herk & K. Landfester, Springer-Verlag, Berlin, 2010, p. 185; b) F. Lan, K.X. Liu, W. Jiang, X.B. Zeng, Y. Wu and Z.-W. Gu, *Nanotechnology*, 2011, **22**, 225604.
- 23 a) V. K. Lamer and R. H. Dinegar, *J. Am. Chem. Soc.*, 1950, **72**, 4847; b) E. Lepeltier, C. Bourgaux, and P. Couvreur, *Adv. Drug Deliver. Rev.*, 2014, **71**, 86.
- 24 F. L. Hatton, P. Chambon, T. O. McDonald, A. Owen and S. P. Rannard, *Chem. Sci.*, 2014, **5**, 1844.
- 25 C. Zhang, V. J. Pansare, R. K. Prud'homme and R. D. Priestley, *Soft Matter*, 2012, **8**, 86.
- 26 H. Lee and R. G. Larson, *J. Phys. Chem. B.*, 2009, **113**, 13202.